DOI: 10.1111/nyas.14855

ORIGINAL ARTICLE

ANNALS OF THE NEW YORK ACADEMY OF SCIENCES

Nanoarchitecture and molecular interactions of epithelial cell junction proteins revealed by super-resolution microscopy

Amna N. Naser | **William Guiler** | **Qun Lu** | **Yan-Hua Chen**

Department of Anatomy and Cell Biology, Brody School of Medicine, East Carolina University, Greenville, North Carolina, USA

Correspondence
Yan-Hua Chen and Qun Lu, Department of Anatomy and Cell Biology, Brody School of Medicine, East Carolina University, Greenville, NC 27834, USA.
Email: cheny@ecu.edu, luq@ecu.edu

Funding information
National Institute of Diabetes and Digestive and Kidney Diseases, Grant/Award Number: NIH DK103166; National Institute of General Medical Sciences, Grant/Award Number: NIH GM146257

Abstract

Epithelial cells are polarized with defined apical tight junctions (TJs), lateral adherens junctions (AJs), and basal integrin–matrix interactions. However, it is increasingly recognized that resident cell junction proteins can be found in varying locations and with previously unrecognized functions. Our study here presents the nanoarchitecture and nanocolocalization of cell junction proteins in culture and tissue by stochastic optical reconstruction microscopy (STORM). The Z-axial view of noncancerous MDCK-II and PZ-HPV-7 cell–cell junctions resolved β-catenin and $p120^{ctn}$ localizations to TJs and AJs, with $p120^{ctn}$ apical to β-catenin and colocalizing with TJ protein claudin-7. More basally, $p120^{ctn}$ and β-catenin become colocalized. This topography was lost in isogenic Ras-transformed MDCK cells and cancerous PC3 cells, where $p120^{ctn}$ becomes basally localized in relation to β-catenin. Claudin-7 gene conditional knockout (cKO) in mice also have altered polarity of $p120^{ctn}$ relative to β-catenin, like that seen in normal-to-cancer cell phenotypic transformation. Additionally, claudin-7 cKO resulted in redistribution and relocalization of other cell junction proteins, including claudin-1, zonula occludens-1, integrin α2, epithelial cell adhesion molecule, and focal adhesion kinase (FAK); specifically, integrin α2 and FAK were observed at the apical–lateral compartment. Our data show that STORM reveals regional cellular junction nanoarchitecture previously uncharacterized, providing new insight into potential *trans*-compartmental modulation of protein functions.

KEYWORDS
β-catenin, cell junctions, claudins, $p120^{ctn}$, STORM imaging, ZO-1

INTRODUCTION

Though it is one of the most common microscopic techniques, conventional light microscopy has a limited temporal resolution of 200–300 nm constrained by its diffraction limit.[1] Owing to this limitation, two molecules can appear to be colocalized even if they are separated by hundreds of nanometers. These distances are not negligible, as they could have important implications when considering whether proteins are in sufficient proximity for molecular interactions. Super-resolution microscopy (SRM) techniques, such as stochastic optical reconstruction microscopy (STORM), offer an experimental strategy to study molecules beyond the light microscopy diffraction limit, to visualize their localization and positional relationships. In STORM, individual fluorophores are repeatedly photoactivated, imaged, and photobleached utilizing photoswitchable fluorophores.[2] A super-resolution image is then reconstructed by merging all the single molecule positions.[3] This technique allows for a lateral (*x*,*y*) resolution of 20 nm and an axial (*z*) resolution of 50 nm.[1] STORM is capable

of multicolor imaging, enabling multiple proteins to be visualized within a single image.[4] Additionally, STORM offers superior resolution power with reduced phototoxicity, when compared to other SRM technologies.[5–8]

Cell–cell junctions link adjacent epithelial cells to each other and are vital for many physiological processes, such as tissue homeostasis, barrier functions, cytoskeleton regulation, cell adhesion, and signaling.[9–11] Cell–cell junctions include tight junctions (TJs), adherens junctions (AJs), gap junctions, and desmosomes.[11] TJs, also called zonula occludens, are the most apical component of cell–cell contact regions; they help maintain tissue homeostasis and cell polarity through barrier and fence functions.[12–14] The catenin family of proteins plays an important role within cell–cell junctions through interactions with cadherin molecules, especially by contributing to AJs and the underlying actin cytoskeleton.[15]

The use of astigmatism-based three-dimensional SRM has demonstrated the close proximity of cadherins to β-catenin and the adherens protein p120^{ctn} (also called catenin delta-1) in normal cells.[16] Through cytoskeletal interactions, catenins function to regulate and coordinate cell–cell adhesion, as well as to modulate small Rho GTPases that induce numerous downstream signaling events.[17,18] β-Catenin is a key player in the canonical WNT signaling pathway, ultimately leading to transcriptional activation of target genes; p120^{ctn} largely functions in stabilizing cadherins in cellular junctions and regulating membrane trafficking.[19,20] It is well-established that both β-catenin and p120^{ctn} bind to classical cadherins, exhibiting colocalization with AJs and participating in adhesion and motility during development and tissue homeostasis.[21] Although studies have shown p120^{ctn} colocalization with claudins to form novel hybrid TJs with AJ organization, the influence of TJ integrity on AJ proteins has not been visualized with light microscopy methods.[22]

Madin–Darby canine kidney (MDCK-II) cells serve as a noncancerous cell control as they are a common model to study epithelia due to their well-defined cell junctions and clear apicobasolateral polarity.[23] Ras-transformed MDCK cells exhibit loss of TJ proteins (occludin, ZO-1, and claudin-1) in the cell–cell contact region, as well as weak expression of E-cadherin.[24] This altered the expression of cell junction proteins and the cancerous nature of these cells isogenic to parental MDCK cells made them a unique model to compare to noncancerous MDCK-II cells.

Claudins, major components of TJs, function in controlling paracellular flux of ions and small molecules by acting as channels or tightening the paracellular pathway.[25–27] Deletion of TJ protein claudin-7 in mice causes cell–matrix loosening, chronic dehydration, induction of epithelial-to-mesenchymal transition (EMT), and severe intestinal defects, including ulcerations, inflammation, hyperplasia, and adenomas, highlighting the importance of claudin-7 in maintaining epithelial integrity.[13,25–30] Integrin α2, involved in regulating cell proliferation and adhesion, interacts and colocalizes with claudin-7, as seen by conventional light microscopy.[25] Deletion of claudin-7 results in altered expression and localization of integrin α2 and disruption of the integrin α2/claudin-1 complex.[25] Focal adhesion kinase (FAK), typically localized with integrins, is predominantly involved in cellular adhesion and cell motility.[31,32] Previous studies utilizing SRM investigated the spatial architecture of focal adhesions and identified protein-specific strata that comprise these integrin-based cell adhesions; however, changes in nanoarchitecture due to loss of cell adhesion proteins have not been examined.[33]

In our study here, we used Nikon- or N-STORM technology to study the nanoarchitecture and molecular interactions of selective cell junction proteins, including β-catenin and p120^{ctn}, in MDCK-II cells, isogenic Ras-transformed MDCK cells (MDCKf3), human prostate epithelial cells (PZ-HPV-7), and human metastatic prostate carcinoma cells (PC3). We found that STORM can reveal previously unspecified changes of topographic relationships of junctional proteins and the potential involvement of TJ protein claudin-7 in controlling the AJ protein nanoarchitectures. We also evaluate junctional proteins in a claudin-7 gene conditional knockout (cKO) mouse model.

MATERIALS AND METHODS

Cell culture

MDCK-II, PZ-HPV-7, and PC3 cells were purchased from ATCC (Manassas, VA, USA). Ras-transformed MDCKf3 cells were generously provided by J. Collard (The Netherlands Cancer Institute, Amsterdam, The Netherlands).[24] Cells were cultured according to ATCC instruction and as described[24] and maintained at 37°C with 5% CO_2 until 80–90% confluent. Cells were split with 0.25% Trypsin-EDTA (Gibco, Gaithersburg, MD, USA) and grown on #1.5 coverslips (Electron Microscopy Sciences, Hatfield, PA, USA) prior to staining.

Mouse tissue isolation

All animal experiments and procedures were approved by the East Carolina University (ECU) Animal Care and Use Committee and conducted in compliance with guidelines from the National Institutes of Health and ECU on laboratory animal care and use. The generation of inducible intestinal-specific claudin-7 gene cKO mice was described previously.[34]

Small intestine was isolated from 3-month-old wild type (control) and claudin-7 cKO mice. Isolated tissues were rinsed in 1× phosphate buffered saline (PBS), transferred to a labeled block containing fresh optimal cutting temperature compound, frozen with 2-methylbutane and dry ice, and stored at −80°C until sectioned.

STORM immunofluorescence

Cells on coverslips were fixed in 4% paraformaldehyde (PFA) at room temperature, then treated with fresh 0.1% sodium borohydride for 7 min. Cells were permeabilized in 0.2% Triton X-100, incubated with 100 mM Glycine, and blocked with 10% bovine serum albumin (BSA) at 37°C. Cells were incubated with the first primary antibody for 1 h, rinsed with PBS, and incubated with the appropriate secondary

TABLE 1 List of antibodies

Antibody	Species	Source/catalog #	Dilution
Primary			
β-catenin	Rabbit	Sigma-Aldrich (C2206)	1:100 (IF)
β-catenin	Mouse	BD Transduction Labs (610153)	1:100 (IF)
Claudin-1	Rabbit	Invitrogen (71-7800)	1:50 (IF)
Claudin-7	Rabbit	Immuno-Biological Laboratories (18875)	1:100 (IF)
Claudin-7	Rabbit	Invitrogen (34-9100)	1:100 (IF)
Claudin-7	Mouse	Invitrogen (37-4800)	1:100 (IF)
E-cadherin	Rat	Invitrogen (13-1900)	1:100 (IF)
EpCAM	Rabbit	Cell Signaling (93790)	1:100 (IF)
Focal adhesion kinase	Rabbit	Cell Signaling (3285S)	1:100 (IF)
Integrin α2	Hamster	Chemicon (CBL1345)	1:100 (IF)
$p120^{ctn}$	Mouse	BD Transduction Labs (610134)	1:100 (IF)
ZO-1	Rat	Invitrogen (41-9776-82)	1:100 (IF)
Secondary			
Atto 488	Goat anti-rabbit	Rockland (611-152-122)	1:500 (IF)
Alexa Fluor 488	Goat anti-rabbit	Invitrogen (A-11008)	1:500 (IF)
Alexa Fluor 488	Goat anti-hamster	Invitrogen (A-21110)	1:500 (IF)
Alexa Fluor 488	Goat anti-mouse	Invitrogen (A-11001)	1:500 (IF)
Alexa Fluor 568	Goat anti-rat	Invitrogen (A-11077)	1:500 (IF)
Alexa Fluor 647	Goat anti-hamster	Invitrogen (A-21451)	1:500 (IF)
Alexa Fluor 647	Goat anti-mouse	Invitrogen (A-21236)	1:500 (IF)
Alexa Fluor 647	Goat anti-rat	Invitrogen (A-21247)	1:500 (IF)
Alexa Fluor 647	Goat anti-rabbit	Invitrogen (A-21244)	1:500 (IF)

antibody for 30 min (Table 1). This process was repeated for the second primary antibody and second secondary antibody for the double staining. Cells were postfixed with 4% PFA. Coverslips were imaged in OXEA buffer (50 mM β-mercaptoethylamine hydrochloride, 77% PBS, 20% Sodium DL-Lactate Solution, and 3% OxyFluor) at 100X using the Nikon Ti2-E inverted microscope with an L-APPS H-TIRF attachment and 4-line LUN-F laser module. Secondary antibody colors were changed for protein pairs throughout experiments to ensure that fluorophore specificity did not have an impact on the data collected. For example, Alexa 488 goat anti-rabbit and Alexa 647 goat anti-mouse were used as secondary antibodies in one experiment, then flipped to Alexa 488 goat anti-mouse and Alexa 647 goat anti-rabbit in another experiment.

Fresh frozen intestinal wild-type (control) and claudin-7 cKO tissues were sectioned, fixed with acetone at −20°C, rinsed with PBS, and assembled in a Sequenza rack with 0.2% Triton X-100. Sections were blocked with 5% BSA, then incubated overnight with respective primary antibodies at 4°C (Table 1). Tissue sections were washed with PBS before 1 h incubation with appropriate secondary antibodies at room temperature. Sections were washed with PBS, postfixed with 4% PFA, washed again with PBS, and mounted with Vectashield (Vector Laboratories, H-1000). Stained tissue slides were then imaged at 100× on N-STORM. Secondary antibodies were changed for protein pairs throughout experiments to ensure that fluorophore specificity did not have an impact on the data collected. Immunostaining for claudin-7 in claudin-7 cKO tissues served as a negative control to ensure antibody and fluorophore specificity.

STORM super-resolution imaging and analysis

X, *y*, and *z* calibrations and chromatic alignments were performed as stated in the NIS-Elements Advanced Research User's Guide menu; briefly, *x*, *y*, and *z* calibrations were completed via analyzing a Z-Series data set to determine the orientation and width of identified molecules. A calibration of Gaussian width in *x* and *y*, as a function of *z* position, was generated using a piezo stage insert to translate diffraction limited spots in the *z* dimension. TetraSpeck beads (100 nm) were used to calibrate the three reporter wavelengths both individually in *x*, *y*, and *z* dimensions, as well as used to correct for chromatic and warp aberrations in the *x*, *y*, and *z* dimensions. The alignment of multicolor asymmetric point spread functions allows for *z* calibration and color correction in the *x*, *y*, and *z* directions.

Three sets of images were taken for each double staining combination in cells and intestinal tissue. Each image consisted of 20,000 frames (10,000 frames per channel). Raw images were collected

with the 3D STORM lens to a back-thinned Princeton Instruments Pro-EM-HS EMCCD 512 × 512 camera and analyzed using Nikon's NIS-Elements software. Images were first analyzed for "blinks," which indicate epifluorescent switching; blink thresholds were standardized to ensure that each image was analyzed equally. Thresholding based on peak intensity height allowed the elimination of potential background staining, as well as reduction of false-positive signals. Processing of blinks generated a reconstructed STORM image from which further analysis was completed.

Within NIS-Elements, the distance between protein pairs and percent of protein overlap within layers was analyzed. The distance between protein signals, referred to as the colocalization, was determined using the Intensity Profile tool. Protein signals located along the cell–cell contact were selectively chosen for distance measurement. One hundred distance measurements were taken for each image and then represented in figures as the mean ± SEM. Using the Cell Count (Molecular Count) function, the exact quantification of each molecule among the Z-stack layers was determined. Since the number of molecules in various cell types is expected to differ, the data were normalized by converting to the percentage within each image. Each layer was then used to determine the amount of overlap (both molecules existing in the same focal plane) between proteins. The degree of overlap was compared between top and bottom layers. Lastly, complete nanocolocalization was defined as signals less than 15 nm apart, at which point, the yellow signals are no longer separated into red and green signals. This was used to determine the number of colocalizations present within each cell type.

Two-dimensional snapshots at various magnifications as well as three-dimensional reconstructions of specific regions of interest, such as the cell–cell junction and the cytoplasm, were taken as representative images for each protein staining combination. Twenty Z-stacks were taken for each protein staining combination (total of 120 Z-stacks) and exported as .nd2 files for analysis of colocalization distance using ImageJ (National Institutes of Health, Bethesda, MD, USA). In ImageJ, a 3D projection to the brightest point was created for each Z-stack and a Gaussian Blur filter was placed over the image. A representative line of best fit through the dots was created to generate a Plot Profile of peak intensities for each channel. The absolute value of the difference between the *x*-value for the peak intensity of each channel was measured as the colocalization or the distance between protein signals. Ten calculated differences for each condition were used to determine average colocalization (distance measurement) of protein pairs. Values in figures were represented as mean ± SEM.

Statistical analysis

Statistical analysis was performed using GraphPad Prism version 8.4.1 for Mac (GraphPad Software, La Jolla, CA, USA). Differences between and among groups were analyzed using the unpaired Student's *t* test and two-way ANOVA. Data were presented as mean ± SEM. A *p* value less than 0.05 was considered statistically significant.

RESULTS

STORM technology allows for visualization of nanolocalization and protein interactions

STORM technology utilizes photoswitchable fluorophores to precisely localize particles.[1,3,4] In conventional microscopy, all fluorophores are activated at once, resulting in a low-resolution image; however, the photoswitchable nature of STORM fluorophores results in high-resolution images (Figure 1A). Figure 1B depicts the series of analytical events that lead to the final reconstructed STORM image. Following data acquisition, a raw STORM image is obtained from which blinks—indicating epifluorescent switching—can be discerned (Figure 1B). The peak intensity of these blinks is used to set a minimum threshold for what NIS-Elements will count as a signal (Figure 1B). The program then analyzes each frame for blinks with a peak intensity higher than the set threshold to create a reconstructed image with the precise localization of the probed proteins (Figure 1B). Blinks represent the certainty of a protein being present in that location. A strong blink corresponds to high probability of a protein being present; therefore, the dot representing this protein in the reconstructed STORM image will be small and pinpointed. Weaker signals will result in larger and more unresolved dots. Since STORM is a three-dimensional super-resolution imaging technique, the obtained image can be viewed in *x*, *y*, and *z* dimensions to ascertain topographical relationships between proteins that otherwise could not be illustrated utilizing conventional microscopy.

SRM technology was utilized to determine the regional architecture of cell–cell junction protein organization in both cells and tissues. Figure 1C depicts a proposed model of regional architecture of AJ proteins β-catenin and $p120^{ctn}$ in normal cultured cells, illustrating where the defined "top" and "bottom" AJ layers are located. In cell experiments, following standard image acquisition through NIS-Elements, a Z-stack was generated for each image and percent overlap of molecules was analyzed (Figure 1D). The Intensity Profile tool was used to measure the distance between protein signals localized to the cell–cell junction that appeared to be closely localized (Figure 1D). For analysis of protein nanolocalization in tissue samples, Z-stacks were generated for each image in NIS-Elements. Files were imported into ImageJ and separated into 3D projections of individual channels (Figure 1E). A Gaussian blur filter was placed over the image and a line of best fit was used to generate a plot profile based on peak intensity (Figure 1E). Colocalization was calculated by taking the absolute value of the peak intensity for the red channel subtracted by the peak intensity for the green channel (Figure 1E).

β-Catenin and $p120^{ctn}$ distribution, colocalization, and nanohierarchical relationship

To examine the nanoarchitectures of β-catenin and $p120^{ctn}$ utilizing N-STORM, noncancerous MDCK-II cells were compared to the

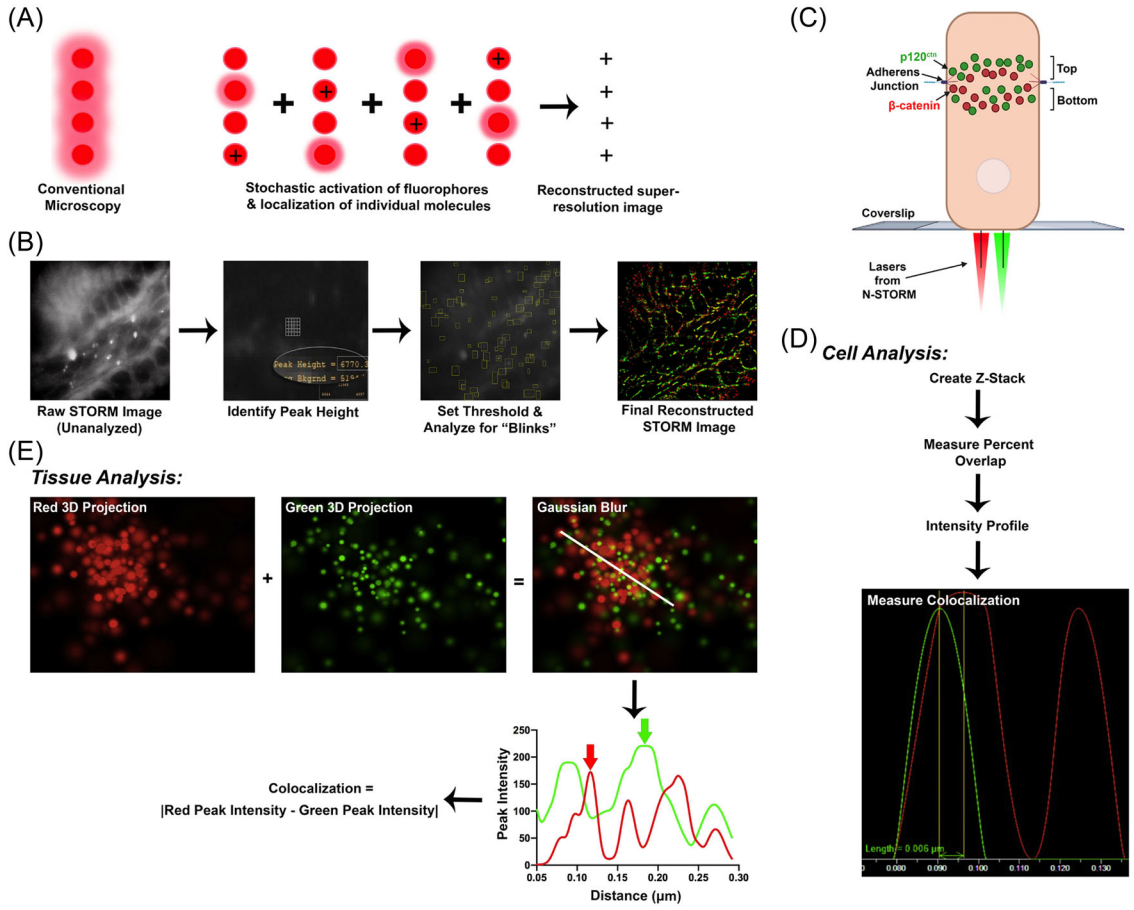

FIGURE 1 Graphic illustrating STORM technology and analyses. (A) Graphic comparison between conventional microscopy and STORM technology; (B) process through which the final reconstructed STORM image is obtained. The representative image is from healthy intestinal tissue in which red represents integrin α2 signal and green marks focal adhesion kinase signal; (C) proposed model of regional architecture of β-catenin and p120^{ctn} depicting "top" and "bottom" layers in relation to the cell. Top corresponds to the apical side, while bottom corresponds to the basolateral side; (D) analysis workflow for cell-based experiments; (E) workflow for analysis completed in tissue-based experiments.

isogenic Ras-transformed MDCKf3 cells, and normal human prostate PZ-HPV-7 cells compared to cancerous prostate PC3 cells. We observed that the localization and distribution of both β-catenin and p120^{ctn} were significantly altered in cancerous cells compared with their healthy counterparts (Figure 2A,D). The high-resolution power and the unique fluorescent signal acquisition–mechanism of STORM allows for the visualization of individual fluorescent dots that represent mostly the labeling of single molecules. This enables clear depiction of protein signals within a region to demonstrate the true distance between signals, rather than an unresolved cluster that would result from conventional microscopy methods (Figure 1A). High magnification view of the cell–cell junction demonstrated significantly increased distance between β-catenin and p120^{ctn} protein signals and their decreased colocalization in MDCKf3 and PC3 cells, compared with their noncancerous counterparts (Figure 2A,D; arrows indicate the cell junction region depicted in the high-resolution insert). The number of colocalizations (signals within 15 nm of each other) present in MDCKf3 and PC3 cells was significantly reduced compared with MDCK-II and PZ-HPV-7 cells (Figure 2B,E). This is also depicted in the high magnification images in which there were fewer instances of yellow dots in MDCKf3 and PC3 cells (Figure 2A,D, bottom panel). Additionally, the mean distance between the STORM signals of β-catenin and p120^{ctn} in MDCKf3 and PC3 cells was significantly larger compared with the distances observed in MDCK-II and PZ-HPV-7 cells (Figure 2C,F). Visually, there was not clear localization of β-catenin and p120^{ctn} to the cell–cell contact region in MDCKf3 cells compared with MDCK-II cells (Figure 2A), consistent with the literature.[24] This finding also further supports the notion that β-catenin redistributes to the cytoplasm and nucleus, carrying signaling functions outside of the cell junction in cancerous cells.[35]

The difference in β-catenin and p120^{ctn} regional nanoarchitecture among layers of the cell–cell junction was also examined. Three-dimensional imaging showed that the top layer corresponds to TJ, or near the TJ level, of the cell, while the bottom layer corresponds to the basolateral level of the AJ. Interestingly, in the top layer of noncancerous cells, β-catenin and p120^{ctn} were separated, with p120^{ctn} localized further toward the TJ at the apical surface (Figure 2G,I); this finding is consistent with the literature highlighting that p120^{ctn} can interact with TJs, whereas β-catenin mainly interacts with AJs.[15,18–29,36] In

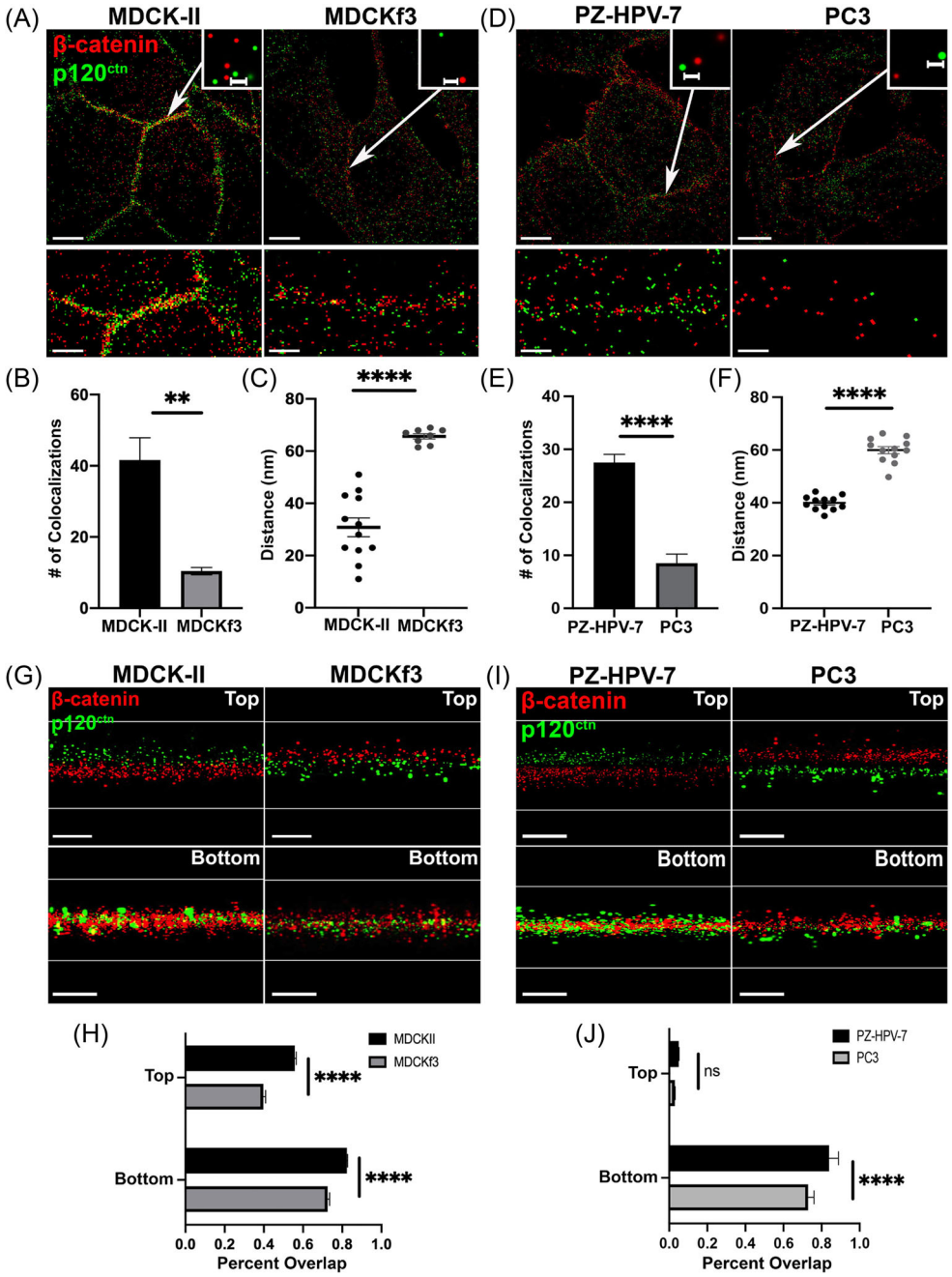

FIGURE 2 STORM imaging highlights significantly reduced nanocolocalization and altered distribution of β-catenin and p120^{ctn} in cancerous cells. (A) β-catenin and p120^{ctn} in MDCK-II and MDCKf3 cells; (B) quantification of colocalizations; (C) quantification of average distance; (D) β-catenin and p120^{ctn} in PZ-HPV-7 and PC3 cells; (E) quantification of colocalizations; (F) quantification of average distance; (G) 3D reconstruction of AJ layers in MDCK-II and MDCKf3 cells; (H) quantification of percent overlap; (I) 3D reconstruction of AJ layers in PZ-HPV-7 and PC3 cells; (J) quantification of percent overlap. The distance between signals, number of colocalizations, and percent overlap were compared by unpaired *t* tests. Inserts of the region indicated by the arrow demonstrate separation of protein signals at high resolution. 2D scale bars: top = 7 μm; bottom = 500 nm; inserts = 20 nm; 3D scale bars = 100 px. $n = 9$. **** $p \leq 0.0001$, ** $p \leq 0.01$, ns $p > 0.05$.

MDCKf3 and PC3 cells, however, this localization of p120^{ctn} toward the apical TJ was lost, as p120^{ctn} was found localized basal to β-catenin (Figure 2G,I). This topographic change was also visualized in videos (see Videos S1 and S2). β-Catenin and p120^{ctn} were largely colocalized in the bottom layer compared to the top layer in all cell lines (Figure 2G,I, bottom panel). Additionally, there was a significant difference in the molecular interactions (degree of overlap) of β-catenin and p120^{ctn} between top and bottom layers in all cell lines, with an increased degree of overlap in the bottom layers (Figure 2H,J). There was also significantly less overlap in the bottom layers of cancerous cells compared with the noncancerous cells (Figure 2H,J). The normal topographical relationship and molecular interactions of β-catenin and p120^{ctn} were evaluated by three-dimensional video of MDCK-II cells (see Video S1); we found an altered organization pattern in MDCKf3 cells (see Video

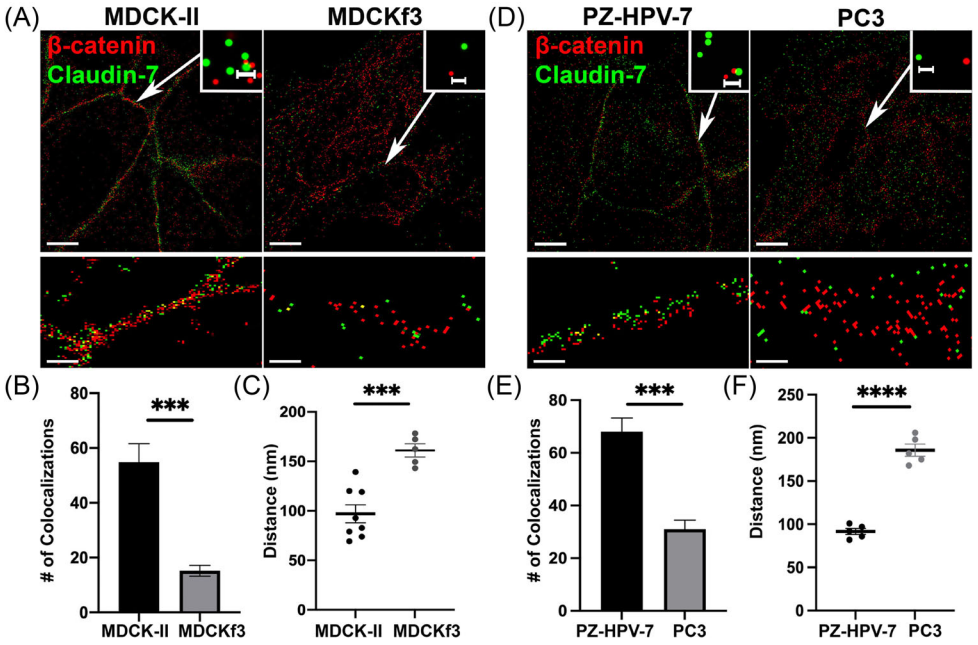

FIGURE 3 Altered distribution and reduced nanocolocalization of β-catenin and claudin-7 in MDCKf3 and PC3 cells. (A) β-catenin and claudin-7 in MDCK-II and MDCKf3; (B) quantification of colocalizations between β-catenin and claudin-7; (C) quantification of average distance between β-catenin and claudin-7; (D) β-catenin and claudin-7 in PZ-HPV-7 and PC3 cells; (E) quantification of colocalizations between β-catenin and claudin-7; (F) quantification of average distance between β-catenin and claudin-7. The distance between signals and number of colocalizations were compared by unpaired *t* test and plotted as mean ± SEM. Inserts of the region indicated by the arrow demonstrate separation of protein signals at high resolution. Scale bars: top = 7 μm; bottom = 500 nm; inserts = 20 nm. $n = 9$. **** $p \leq 0.0001$, *** $p \leq 0.001$.

S2), with loss of p120^{ctn} apical position in relation to β-catenin. This topographic change of p120^{ctn} localization may suggest the disruption of TJs and AJs connection in cancerous cells.

Claudin-7 distribution and colocalization with p120^{ctn} altered in cancerous cells

The observation of p120^{ctn} localization apical to β-catenin prompted us to investigate the topographic relationship among other AJ and TJ proteins. TJ protein claudin-7 was found to be coimmunostained with β-catenin in MDCK-II and PZ-HPV-7 cells but not in MDCKf3 and PC3 cells. Two-dimensional STORM revealed an altered nanoarchitecture of β-catenin and claudin-7 in MDCKf3 and PC3 cells, as the normal β-catenin and claudin-7 localization in MDCK-II and PZ-HPV-7 cells to the cell–cell junction (Figure 3A,D, left panel, bottom image shows the high magnification) was largely disrupted (Figure 3A,D, right panel, bottom image shows the high magnification). High-resolution depiction of cell–cell junctions demonstrated decreased protein localization at the cell junction and increased distance between protein signals in MDCKf3 and PC3 cells (Figure 3A,D; arrows indicate the region depicted in the high-resolution insert). Quantitatively, there were significantly fewer colocalizations, as well as increased distance between signals in MDCKf3 cells compared with MDCK-II cells (Figure 3B,C); this decreased colocalization and increased distance between signals were also observed in PC3 cells (Figure 3E,F).

Previous studies highlighted p120^{ctn} interaction with claudins to form a novel hybrid TJ structure.[22] We evaluated this by coimmunostaining for claudin-7 and p120^{ctn} and visualizing at the super-resolution level. As previously reported, p120^{ctn} and claudin-7 exhibited strong distribution at the cell–cell junction as well as high colocalization in MDCK-II and PZ-HPV-7 cells (Figure 4A,D, left panel; bottom panel, high magnification; high-resolution inserts demonstrate nanocolocalization of these proteins). In contrast, MDCKf3 and PC3 cells exhibited disorganized cell–cell junctions with diminished colocalization of p120^{ctn} and claudin-7 (Figure 4A,D, right panel; bottom panel, high magnification). There were both significantly fewer colocalizations of p120^{ctn} and claudin-7 and increased average distance in MDCKf3 and PC3 cells, compared with MDCK-II and PZ-HPV7 cells (Figure 4B,C and E,F). This suggests that p120^{ctn} interaction with TJ proteins is lost in cancerous cells.

TJ and AJ protein colocalization is disrupted in claudin-7 cKO intestinal tissue

To investigate the effect of TJ protein deficiency on AJ protein organization, we next explored the nanoarchitecture of TJ and AJ proteins at the tissue level, utilizing an inducible intestine-specific claudin-7 cKO model. β-Catenin and p120^{ctn} were double labeled in control and cKO intestinal tissues and examined by N-STORM.

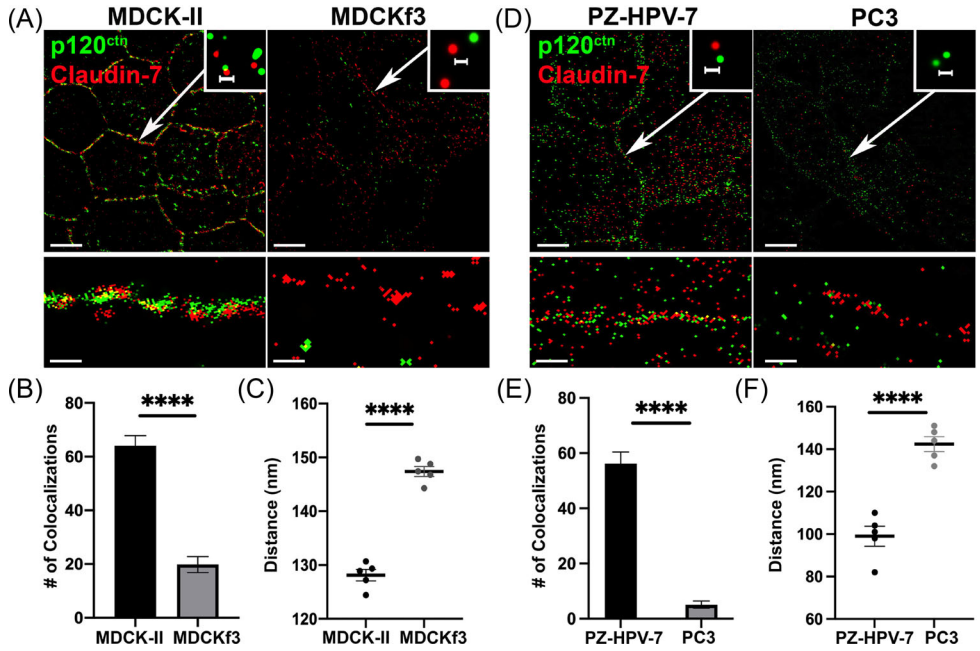

FIGURE 4 Disrupted distribution and reduced nanocolocalization of p120^{ctn} and claudin-7 in MDCKf3 and PC3 cells. (A) p120^{ctn} and claudin-7 in MDCK-II and MDCKf3 cells; (B) quantification of colocalizations; (C) quantification of average distance. (D) p120^{ctn} and claudin-7 in PZ-HPV-7 and PC3 cells; (E) quantification of colocalizations; (F) quantification of average distance. The distance between signals and number of colocalizations were compared by unpaired *t* test and plotted as mean ± SEM. Inserts of the region indicated by the arrow demonstrate separation of protein signals at high resolution. Scale bars: top = 7 μm; bottom = 500 nm; inserts = 20 nm. $n = 9$. **** $p \leq 0.0001$.

Two-dimensional imaging of β-catenin and p120^{ctn} in control and cKO intestinal tissues revealed significant differences in organization and nanocolocalization (Figure 5). In control tissue, β-catenin and p120^{ctn} were organized in nanoclusters along the cell–cell junction (Figure 5A, left panel; arrows indicate cell–cell junctions). β-Catenin and p120^{ctn} were more disorganized in claudin-7 cKO tissues, exhibiting decreased localization to the cell–cell junction (Figure 5A, right panel; arrowheads indicate random nonjunctional distribution).

Three-dimensional imaging highlighted the localization of β-catenin and p120^{ctn} both at the cell–cell junction and in the cytoplasm (Figure 5B), supporting previous hypotheses that β-catenin and p120^{ctn} may participate in cellular functions in nonjunctional locations.[35,37] Junctional 3D images highlighted discernible nanoclusters of β-catenin and p120^{ctn}, as well as p120^{ctn} localization to the apical side in reference to β-catenin and more basal localization in cKO tissues (Figure 5B, top row; arrows indicate apical localization in control, whereas arrowheads indicate basolateral localization in cKO). This observation substantiated the altered nanoarchitecture of β-catenin and p120^{ctn} from noncancerous to cancerous cells in culture, in that TJ protein disruption is sufficient to promote p120^{ctn} redistribution from apical to basal of β-catenin. Quantitative analysis revealed a significant difference in the average colocalization (distance between protein signals) between β-catenin and p120^{ctn} in control versus cKO (Figure 5C). These results indicate that deletion of claudin-7 in intestines disrupts the nanocolocalization of β-catenin and p120^{ctn} at the cell–cell junction and shifts p120^{ctn} position from apical to basal of β-catenin.

Previous studies demonstrated that the TJ structure remains intact in claudin-7 KO intestinal epithelial cells as revealed by transepithelial resistance measurement.[25] To determine whether the TJ protein organization also remains unaffected in claudin-7 cKO intestinal epithelia, the effect of claudin-7 deletion on other TJ proteins was examined by double labeling claudin-1 and ZO-1 in intestinal tissue using the STORM technology. Claudin-1 is vital in maintaining TJ integrity as its deletion in mice leads to severe water loss and dehydration resulting in death within 1 day.[38,39] ZO-1 acts as a scaffolding protein to cross-link and anchor TJ proteins to the actin cytoskeleton.[40] As anticipated, control tissues exhibited colocalization of ZO-1 and claudin-1 along the cell membrane (Figure 5D, left panel; arrows, yellow signals indicate colocalization). In contrast, significantly less colocalization of ZO-1 and claudin-1 and disrupted cell–cell junctions were observed in claudin-7 cKO tissues (Figure 5D, right panel; arrowheads, red signal clusters are separated from the green signals).

Three-dimensional examination of cell junctions versus the cytoplasm revealed similar findings. ZO-1 and claudin-1 were highly nanocolocalized at the cell–cell junction of control tissues, as indicated by concentrated clustering and yellow color due to signal overlap; in contrast, in the cKO intestinal tissues, ZO-1 and claudin-1 were found frequently separated from each other (Figure 5E, top row). Visually, there was also increased distance between ZO-1 and claudin-1 signals in cKO tissues (Figure 5D), which was confirmed by quantification of distance measurements (Figure 5F). In addition, the expression of ZO-1 was increased in the cytoplasm of claudin-7 cKO tissues (Figure 5E, bottom row), suggesting that claudin-7 cKO may cause altered localization of ZO-1, leading to increased concentration in the cytoplasm.

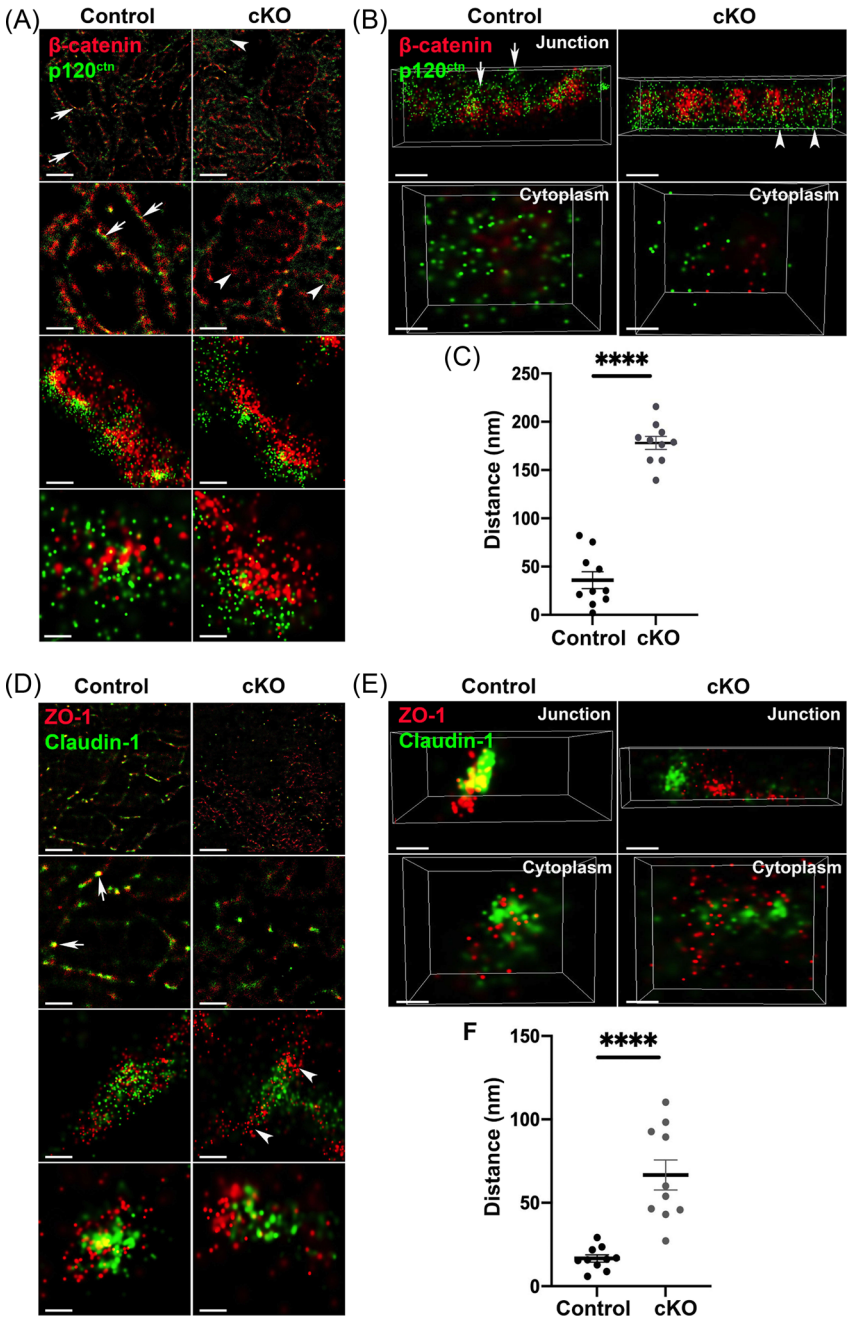

FIGURE 5 Significantly reduced colocalization of β-catenin and p120^{ctn} and disrupted claudin-1 and ZO-1 localization in claudin-7 cKO intestinal tissues. (A) Two-dimensional snapshots of β-catenin and p120^{ctn}. Arrows: cell–cell junction; arrowheads: random nonjunctional distribution. (B) Three-dimensional snapshots of β-catenin and p120^{ctn} at the cell junction and cytoplasm. Arrows: apical localization of p120^{ctn}; arrowheads: basolateral localization of p120^{ctn} in claudin-7 knockout intestines. (C) Quantification of average distance. (D) Two-dimensional snapshots of ZO-1 and claudin-1; arrows: colocalization of ZO-1 and claudin-1; arrowheads: displacement of ZO-1 from claudin-1. (E) Three-dimensional snapshots of ZO-1 and claudin-1 at the junction and cytoplasm. (F) Quantification of average distance. The distance between signals was compared by unpaired *t* test and plotted as mean ± SEM. 2D scale bars (top to bottom) = 5 μm, 2.5 μm, 500 nm, 250 nm; 3D scale bars = 100 px. $n = 10$. $^{****}p \leq 0.0001$.

Claudin-7 cKO leads to disruption of integrin α2, FAK, and EpCAM

The distance hierarchal relationship among β-catenin, p120^{ctn}, claudin-7, claudin-1, and ZO-1 raised questions about effects on other junctional protein topographical organization. Our previous study demonstrated that claudin-7 is not only localized at apical TJs but also distributed along the basolateral surface, where it interacts with integrin α2.[25] Deletion of claudin-7 in mouse intestines disrupts cell–matrix interactions.[25]

Therefore, we stained control and claudin-7 cKO tissues for integrin α2, claudin-7, FAK, and epithelial cellular adhesion molecule (EpCAM). Claudin-7 was highly colocalized with integrin α2 in the control intestinal tissue, measured to be on average 40.17 ± 19.37 nm apart (Figure 6A, left panel; arrows indicate colocalization at cell–cell junctions). Similarly, claudin-7 colocalized with FAK, with peak intensity measurements of 49.42 ± 35.50 nm apart (Figure 6B, left panel; arrows indicate colocalization at cell–cell junctions). In contrast, colocaliztion of integrin α2 and FAK was disrupted in claudin-7 cKO (Figure 6A,B, right panel). Three-dimensional analysis confirmed discontinuous integrin α2 distribution at the cell junction in cKO intestinal tissues (Figure 6C, top panel). Control tissues exhibited relatively uniform integrin α2 along the junction; however, there was more clustering of integrin α2 signal in the junction of cKO tissues (Figure 6C, top panel). Integrin α2 was present in the cytoplasm in both control and cKO (Figure 6C, bottom panel). FAK was localized to the

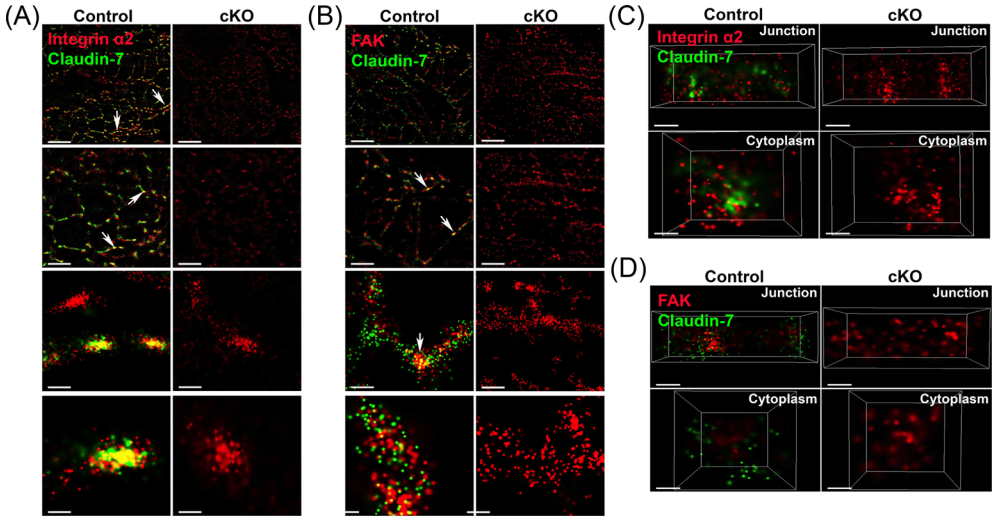

FIGURE 6 Disruption of integrin α2 and FAK organization due to loss of claudin-7 in intestine. (A) Two-dimensional snapshots of integrin α2 and claudin-7. (B) Two-dimensional snapshots of FAK and claudin-7. (C) Three-dimensional snapshots of integrin α2 and claudin-7. (D) Three-dimensional snapshots of FAK and claudin-7. Arrows: cell–cell junctions. 2D scale bars (top to bottom) = 5 μm, 2.5 μm, 500 nm, 250 nm; 3D scale bars = 100 px. $n = 10$.

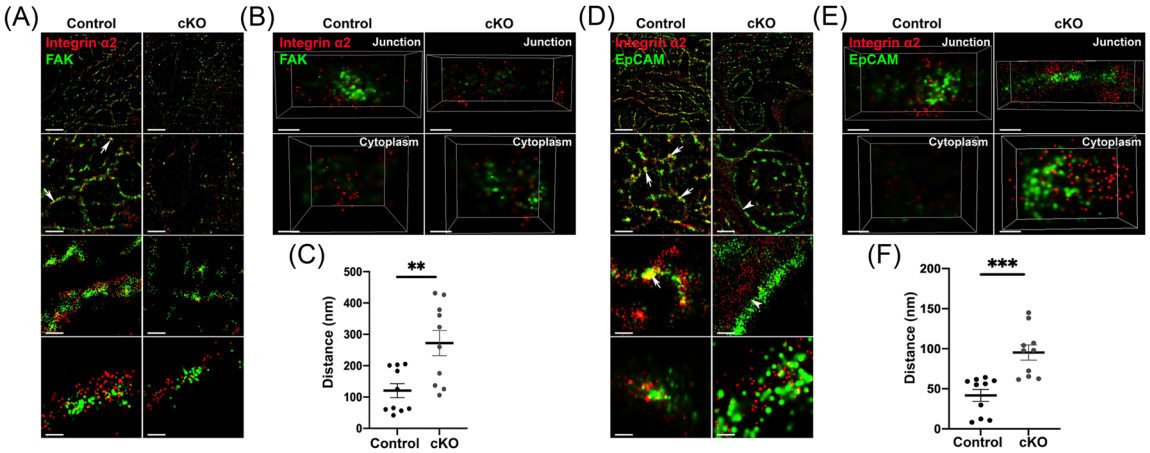

FIGURE 7 Altered integrin α2, FAK, and EpCAM localization in claudin-7 cKO intestinal tissues. (A) Two-dimensional snapshots of integrin α2 and FAK; (B) three-dimensional snapshots of integrin α2 and FAK; (C) quantification of average distance between integrin α2 and FAK; (D) two-dimensional snapshots of integrin α2 and EpCAM; (E) three-dimensional snapshots of integrin α2 and EpCAM; (F) quantification of average distance between integrin α2 and EpCAM. The distance between signals was compared by unpaired *t* test and plotted as mean ± SEM. Arrows: cell–cell junctions; arrowheads: separation of signals at cell junction. 2D scale bars (top to bottom) = 5 μm, 2.5 μm, 500 nm, 250 nm; 3D scale bars = 100 px. $n = 10$. $^{***}p \leq 0.001$, $^{**}p \leq 0.01$.

cell–cell junction in relation to claudin-7 (Figure 6D, top panel); cKO tissues exhibited significantly increased cytoplasmic FAK and random distribution within the cells (Figure 6B,D, right panel).

Investigation into the interaction between FAK and integrin α2 yielded similar results. Control tissues exhibited highly organized protein localization along the cell–cell junction (Figure 7A, left panel; arrows indicate cell–cell junctions). However, colocalization of integrin α2 and FAK was disrupted in cKO tissues (Figure 7A, right panel). Three-dimensional STORM revealed decreased FAK expression along the cell junction in cKO intestines, as well as increased FAK expression in the cytoplasm compared with control tissues (Figure 7B). The distance between integrin α2 and FAK signals was found to be significantly higher in claudin-7 cKO tissue (Figure 7C).

Additionally, integrin α2 and EpCAM were highly nanocolocalized at the cell junction in control tissues (Figure 7D, left panel; arrows depict colocalization at the junction). In contrast, cKO tissues exhibit disorganized integrin α2 colocalization (Figure 7D, right panel) and EpCAM. Similar to two-dimensional examination, three-dimensional

analysis of integrin α2 and EpCAM in control tissue showed integrin α2 localized closely with EpCAM at the cell–cell junction; however, the two proteins were separated (both above and below) in cKO tissues (Figure 7E, top panel). Additionally, there was increased cytoplasmic integrin α2 and EpCAM in cKO intestinal tissues, compared with control tissue (Figure 7E, bottom panel). Analysis of nanocolocalization also demonstrated a significantly increased distance between integrin α2 and EpCAM in claudin-7 cKO intestines (Figure 7F).

DISCUSSION

Conventional microscopy has established that β-catenin and p120^{ctn} are associated with AJs. Molecular studies have also confirmed that β-catenin binds to the carboxyl terminus of p120^{ctn} and interacts with the juxtamembrane domain on classical cadherins.[19,20,36,41,42] By using N-STORM, the present study supports results in the published literature, but also provides new data that may have important implications.

N-STORM investigation into the protein localization in the cell–cell contact area revealed, for the first time, a topographical relationship among catenin molecules that was not reported before by conventional microscopy. We observed that p120^{ctn} is localized apical to β-catenin in a hierarchal topography of AJs and TJs, although they are largely colocalized in AJs in MDCK-II and PZ-HPV-7 cells. This spatial organization is altered in the isogenic Ras-transformed MDCKf3 cells and cancerous PC3, in that the p120^{ctn} localization became basal to β-catenin (Figure 2G,I; and Videos S1 and S2). Furthermore, for mouse intestinal epithelial tissues, where p120^{ctn} is not downregulated as it is in MDCKf3 and PC3 cells, p120^{ctn} redistribution to the basal side in reference to β-catenin is likewise quite clear when claudin-7 is deleted in the cKO mice (Figure 5B). These findings showed that the removal of the TJ integral membrane protein claudin-7 is sufficient to alter the p120^{ctn}–β-catenin topographical relationship. Currently, it is not known whether this displacement of p120^{ctn} contributes to the invasive properties of cancerous cells. The disorganization of p120^{ctn} in claudin-7 cKO mouse intestinal epithelium suggests that claudin-7 is essential in maintaining topographical relationships between AJ proteins and that p120^{ctn} likely has different pools, with some being intimately involved in TJ organization and function. Smalley-Freed *et al.* reported that p120^{ctn} conditional deletion leads to abnormal barrier function, increased inflammation, and disrupted epithelial homeostasis and survival in the intestine.[43] It is possible that the reduction of p120^{ctn} expression or its altered distribution in cancerous cells may contribute to the weakening of both TJs and AJs during EMT. We have previously reported that TJs form before AJs in Ras-transformed epithelial cells when the cancer-like cells reestablish cell–cell junctions after PD98095 treatment.[24] Additionally, downregulation of claudin-7 induces colorectal cancer metastasis and invasion through promotion of EMT.[14] Taken together, our results are consistent with the literature and highlight the potential roles of TJ proteins in influencing the nanoarchitecture and localization of AJ proteins in cancerous cells.

However, it is worth pointing out that our current study is based on mature junctions. It is unclear whether p120^{ctn} and β-catenin have the same topographical relationship during the assembly of junctions when using a calcium switch assay. A recent study by Beggs *et al.* indicates that desmoplakin protein goes through an architectural change during desmosome assembly using direct stochastic optical reconstruction microscopy.[44] This finding suggests that some junctional proteins undergo dynamic organizational changes over the course of junctional assembly and maturation processes.

Compared with conventional light microscopy, SRM, such as N-STORM, allows the determination of protein–protein topographical relationships on the nanometer scale. Another interesting finding of the present study is that the average distances between AJ proteins (~70 nm) in a cancerous cell never become greater than that between AJ and TJ proteins of a noncancerous cell (~100 nm). These data indicated that AJ proteins that interact with each other in noncancerous cells remain physically close even in transformed cancerous cells. Although the biological significances are not known, one may speculate that in embryogenesis or cancer development, an EMT process routinely progresses to mesenchymal-to-epithelial transition.[45] The residual expression of cell–cell junction proteins following EMT may act as seeds that can quickly reassemble when they remain close to AJ and TJ organization. Future studies using real-time video imaging with experimental interventions may shed light on the functions of this topographical protein positioning.

In intestinal tissues, we found β-catenin and p120^{ctn} also to be highly nanocolocalized at the cell–cell junction; however, localization at the cell junction was disrupted claudin-7 cKO tissue. Discernable nanoclusters of β-catenin and p120^{ctn} signals in the cytoplasm further support the idea that these proteins play other important roles outside of the cell junction.[19,35,46] β-Catenin is involved in WNT signaling from the plasma membrane to the nucleus;[37] this function explains the ubiquitous expression of β-catenin throughout the cell, especially since this distribution was not associated with p120^{ctn}. Previous studies reported that p120^{ctn} may regulate WNT signaling–mediated nuclear transcription through Kaiso.[46] Further studies are needed to decipher the exact nature of p120^{ctn}'s role and how it performs functions with β-catenin interactions at the cell–cell junction, but without it in WNT signaling.

Previous studies have suggested an important interaction between claudin-7 and integrin α2 to form a functional complex.[25] There is increasing evidence suggesting that integrins accumulate in the apical compartment in which they interact with TJ proteins and connexins.[47] Our use of N-STORM confirmed the colocalization of claudin-7 and integrin α2 and examined the nanoscale molecular architecture of integrin α2. Among claudin-7 cKO tissues, integrin α2 exhibited altered expression and nonhomogeneous distribution, as integrin α2 was largely found outside of the junction. Similarly, EpCAM showed clear dissociation at the cell–cell junction in claudin-7 cKO intestines. FAK organization was also disrupted in claudin-7 cKO intestinal tissues. Investigation into the interaction of claudin-7 with focal adhesion structures suggested the localization of claudin-7 between integrin α2 and FAK, with preference toward the side of integrin α2 (Figure 6, 40.17 ± 19.37 nm vs. 49.42 ± 35.50 nm). It is worth indicating that not only integrin α2 and EpCAM, but some FAK, also localized at apical side of cell junctions and interacted with claudin-7, a result owing to the

fact that N-STORM imaging can only be focused on the apical region. In control intestinal tissues, claudin-1 and ZO-1 are highly colocalized at the cell–cell junction; however, the deletion of claudin-7 resulted in significantly increased distance between STORM signals. These results suggest that claudin-7 may play a regulatory role in cell–cell junction composition, as claudin-7 cKO leads to the displacement of many cell junction proteins.

The use of STORM technology to reveal the regional architecture of cell–cell junction proteins in tissues, as well as comparison of non-cancerous and cancerous cells, is an example of how new technology can improve the understandings of protein interactions and functions. In addition, previous data can be re-examined using SRM technology. However, although STORM technology is very powerful, it will not be able to fully eliminate other methods, such as the protein complex immunoprecipitation assays. STORM can evaluate proteins *in situ* and the close localization of two proteins at the nanoscale level. On the other hand, an immunoprecipitation assay requires disruption of the cell membrane and relies on the physical interaction between the molecules, which does not necessarily mean that only two proteins are interacting with each other. We envisage that STORM technology will be a complementary method to other biochemical assays.

ACKNOWLEDGMENTS

The authors thank Joani Zary Oswald and Christi Boykin for their technical assistance. This study was funded by NIH DK103166 and NIH GM146257.

AUTHOR CONTRIBUTIONS

A.N. performed all tissue-based experiments and cell imaging, collected and analyzed data, formulated figures, and wrote the first draft of the manuscript. W.G. performed cell-based experiments. Q.L. conceptualized and supervised the study, interpreted data, and edited the manuscript. Y.-H.C. conceptualized and supervised the study, interpreted data, and finalized the manuscript.

COMPETING INTERESTS

The authors declare no competing interests.

PEER REVIEW

The peer review history for this article is available at: https://publons.com/publon/10.1111/nyas.14855.

REFERENCES

1. Xu, J., Ma, H., & Liu, Y. (2017). Stochastic optical reconstruction microscopy (STORM). *Current Protocols in Cytometry*, *81*, 12.46.1–12.46.27.
2. Lin, D., Gagnon, L. A., Howard, M. D., Halpern, A. R., & Vaughan, J. C. (2018). Extended-depth 3D super-resolution imaging using probe-refresh STORM. *Biophysical Journal*, *114*(8), 1980–1987.
3. Quang, B. A., & Lenne, P. F. (2015). Superresolution measurements in vivo: Imaging Drosophila embryo by photoactivated localization microscopy. *Methods in Cell Biology*, *125*, 119–142.
4. Tam, J., & Merino, D. (2015). Stochastic optical reconstruction microscopy (STORM) in comparison with stimulated emission depletion (STED) and other imaging methods. *Journal of Neurochemistry*, *135*(4), 643–658.
5. Hell, S. W., & Wichmann, J. (1994). Breaking the diffraction resolution limit by stimulated emission: Stimulated-emission-depeletion fluorescence microscopy. *Optics Letters*, *19*(11), 780–782.
6. Gustafsson, M. G. L. (2000). Surpassing the lateral resolution limit by a factor of two using structured illumination microscopy. *Journal of Microscopy*, *198*(2), 82–87.
7. Hein, B., Willig, K. I., & Hell, S. W. (2008). Stimulated emission depletion (STED) nanoscopy of a fluorescent protein-labeled organelle inside a living cell. *Proceedings of the National Academy of Sciences of the United States of America*, *105*(38), 14271–14276.
8. Demmerle, J., Innocent, C., North, A. J., Ball, G., Müller, M., Miron, E., Matsuda, A., Dobbie, I. M., Markaki, Y., & Schermelleh, L. (2017). Strategic and practical guidelines for successful structured illumination microscopy. *Nature Protocols*, *12*(5), 988–1010.
9. Sluysmans, S., Vasileva, E., Spadaro, D., Shah, J., Rouaud, F., & Citi, S. (2017). The role of apical cell–cell junctions and associated cytoskeleton in mechanotraduction. *Biologie Cellulaire*, *109*(4), 139–161.
10. Friedl, P., & Mayor, R. (2017). Tuning collective cell migration by cell–cell junction regulation. *Cold Spring Harbor Perspectives in Biology*, *9*(4), a029199.
11. Garcia, M. A., Nelson, W. J., & Chavez, N. (2018). Cell–cell junctions organize structural and signaling networks. *Cold Spring Harbor Perspectives in Biology*, *10*(4), a029181.
12. Lu, Z., Ding, L., Lu, Q., & Chen, Y.-H. (2013). Claudins in intestines: Distribution and functional significance in health and diseases. *Tissue Barriers*, *1*(3), e24978.
13. Wang, K., Xu, C., Li, W., & Ding, L. (2018). Emerging clinical significance of claudin-7 in colorectal cancer: A review. *Cancer Management and Research*, *10*, 3641–3752.
14. Wang, K., Li, T., Xu, C., Ding, Y., Li, W., & Ding, L. (2019). Claudin-7 down-regulation induces metastasis and invasion in colorectal cancer via the promotion of epithelial-mesenchymal transition. *Biochemical and Biophysical Research Communications*, *508*(3), 797–804.
15. Nagafuchi, A. (2001). Molecular architecture of adherens junctions. *Current Opinion in Cell Biology*, *13*(5), 600–603.
16. Bertocchi, C., Wang, Y., Ravasio, A., Hara, Y., Wu, Y., Sailov, T., Baird, M. A., Davidson, M. W., Zaidel-Bar, R., Toyama, Y., Ladoux, B., Mege, R.-M., & Kanchanawong, P. (2017). Nanoscale architecture of cadherin-based cell adhesions. *Nature Cell Biology*, *19*(1), 28–37.
17. Reynolds, A. B. (2007). $P120^{ctn}$: Past and present. *Biochimica et Biophysica Acta*, *1773*(1), 2–7.
18. Meng, W., & Takeichi, M. (2009). Adherens junction: Molecular architecture and regulation. *Cold Spring Harbor Perspectives in Biology*, *1*(6), a002899.
19. Anastasiadis, P. Z., & Reynolds, A. B. (2000). The p120 catenin family: Complex roles in adhesion, signaling and cancer. *Journal of Cell Science*, *113*(8), 1319–1334.
20. Tortelote, G. G., Reis, R. R., De Almeida Mendes, F., & Abreu, J. G. (2017). Complexity of the WNT/β-catenin pathway: Searching for an activation model. *Cell Signal*, *40*, 30–43.
21. Mccrea, P. D., & Gu, D. (2010). The catenin family at a glance. *Journal of Cell Science*, *123*(5), 637–642.
22. Nunes, F. D., Lopez, L. N., Lin, H. W., Davies, C., Azevedo, R. B., Gow, A., & Kachar, B. (2006). Distinct subdomain organization and molecular composition of a tight junction with adherens junction features. *Journal of Cell Science*, *119*(23), 4819–4827.
23. Dukes, J. D., Whitley, P., & Chalmers, A. D. (2011). The MDCK variety pack: Choosing the right strain. *BMC Cell Biology [Electronic Resource]*, *12*, 43.
24. Chen, Y.-H., Lu, Q., Schneeberger, E. E., & Goodenough, D. A. (2000). Restoration of tight junction structure and barrier function by down-regulation of the mitogen-activated protein kinase pathway in

Ras-transformed Madin–Darby canine kidney cells. *Molecular Biology of the Cell*, *11*(3), 849–862.
25. Ding, L., Lu, Z., Foreman, O., Tatum, R., Lu, Q., Renegar, R., Cao, J., & Chen, Y.-H. (2012). Inflammation and disruption of the mucosal architecture in claudin-7 deficient mice. *Gastroenterology*, *142*(2), 305–315.
26. Ding, L., Lu, Z., Lu, Q., & Chen, Y.-H. (2013). The claudin family of proteins in human malignancy: A clinical perspective. *Cancer Management and Research*, *5*, 267–275.
27. Xing, T., Camacho Salazar, R., & Chen, Y.-H. (2017). Animal models for studying epithelial barriers in neonatal necrotizing enterocolitis, inflammatory bowel disease, and colorectal cancer. *Tissue Barriers*, *5*(4), e1356901.
28. Lu, Z., Kim, D. H., Fan, J., Lu, Q., Verbanac, K., Ding, L., Renegar, R., & Chen, Y.-H. (2015). A non-tight junction function of claudin-7 – Interaction with integrin signaling in suppressing lung cancer cell proliferation and detachment. *Molecular Cancer*, *14*, 120.
29. Li, W.-J., Xu, C., Wang, K., Li, T.-Y., Wang, X.-N., Yang, H., Xing, T., Li, W.-X., Chen, Y.-H., Gao, H., & Ding, L. (2018). Severe intestinal inflammation in the small intestine of mice induced by controllable deletion of claudin-7. *Digestive Diseases and Sciences*, *63*(5), 1200–1209.
30. Xu, C., Wang, K., Ding, Y. u-H., Li, W.-J., & Ding, L. (2019). Claudin-7 gene knockout causes destruction of intestinal structure and animal death in mice. *World Journal of Gastroenterology*, *25*(5), 584–599.
31. Mitra, S. K., Hanson, D. A., & Schlaepfer, D. D. (2005). Focal adhesion kinase: In command and control of cell motility. *Nature Reviews Molecular Cell Biology*, *6*(1), 56–68.
32. Schaller, M. D. (2010). Cellular functions of FAK kinases: Insight into molecular mechanisms and novel functions. *Journal of Cell Science*, *123*(7), 1007–1013.
33. Kanchanawong, P., Shtengel, G., Pasapera, A. M., Ramko, E. B., Davidson, M. W., Hess, H. F., & Waterman, C. M. (2010). Nanoscale architecture of integrin-based cell adhesions. *Nature*, *468*(7323), 580–584.
34. Xing, T., Benderman, L. J., Sabu, S., Parker, J., Yang, J., Lu, Q., Ding, L., & Chen, Y.-H. (2020). Tight junction protein claudin-7 is essential for intestinal epithelial stem cell self-renewal and differentiation. *Cellular and Molecular Gastroenterology and Hepatology*, *9*(4), 641–659.
35. Valenta, T., Hausmann, G., & Basler, K. (2012). The many faces and functions of β-catenin. *Embo Journal*, *31*(12), 2714–2736.
36. Gu, C., Liu, M., Zhao, T., Wang, D., & Wang, Y. (2015). Protective role of p120-catenin in maintaining the integrity of adherens and tight junctions in ventilator-induced lung injury. *Respiratory Research*, *16*(1), 58.
37. Mccrea, P. D., & Gottardi, C. J. (2016). Beyond β-catenin: Prospects for a larger catenin network in the nucleus. *Nature Reviews Molecular Cell Biology*, *17*(1), 55–64.
38. Furuse, M., Hata, M., Furuse, K., Yoshida, Y., Haratake, A., Sugitani, Y., Noda, T., Kubo, A., & Tsukita, S. (2002). Claudin-based tight junctions are crucial for the mammalian epidermal barrier: A lesson from claudin-1 deficient mice. *Journal of Cell Biology*, *156*(6), 1099–1111.
39. Bergmann, S., Von Buenau, B., Vidal-Y-Sy, S., Haftek, M., Wladykowski, E., Houdek, P., Lezius, S., Duplan, H., Bäsler, K., Dähnhardt-Pfeiffer, S., Gorzelanny, C., Schneider, S. W., Rodriguez, E., Stölzl, D., Weidinger, S., & Brandner, J. M. (2020). Claudin-1 decrease impacts epithermal barrier function in atopic dermatitis lesions dose-dependently. *Science Reports*, *10*(1), 2024.
40. Van Itallie, C. M., Fanning, A. S., Bridges, A., & Anderson, J. M. (2009). ZO-1 stabilizes the tight junction solute barrier through coupling to the perijunctional cytoskeleton. *Molecular Biology of the Cell*, *20*(17), 3930–3940.
41. Lu, Q. (2010). Delta-catenin dysregulation in cancer: Interactions with E-cadherin and beyond. *Journal of Pathology*, *222*(2), 119–123.
42. Liu, N., Li, A. L., Zhou, X. P., Chen, Q., & Cao, W. (2015). P120 catenin attenuates lipopolysaccharide-induced blood–brain barrier dysfunction and inflammatory responses in human brain microvascular endothelial cells. *International Journal of Clinical and Experimental Pathology*, *8*(4), 4202–4212.
43. Smalley-Freed, W. G., Efimov, A., Burnett, P. E., Short, S. P., Davis, M. A., Gumucio, D. L., Washington, M. K., Coffey, R. J., & Reynolds, A. B. (2010). p120-catenin is essential for maintenance of barrier function and intestinal homeostasis in mice. *Journal of Clinical Investigation*, *120*(6), 1824–1835.
44. Beggs, R. R., Rao, T. C., Dean, W. F., Kowalczyk, A. P., & Mattheyses, A. L. (2022). Desmosomes undergo dynamic architectural changes during assembly and maturation. *Tissue Barriers*, 2017225. https://doi.org/10.1080/21688370.2021.2017225
45. Kim, D. H., Xing, T., Yang, Z., Dudek, R., Lu, Q., & Chen, Y.-H. (2017). Epithelial mesenchymal transition in embryonic development, tissue repair and cancer: A comprehensive overview. *Journal of Clinical Medicine*, *7*(1), 1.
46. Daniel, J. M. (2007). Dancing in and out of the nucleus: P120-catenin and the transcription factor Kaiso. *Biochimica et Biophysica Acta*, *1773*(1), 59–68.
47. Peterson, R. J., & Koval, M. (2021). Above the matrix: Functional roles for apically localized integrins. *Frontiers in Cell and Developmental Biology*, *9*, 699407.

SUPPORTING INFORMATION

Additional supporting information can be found online in the Supporting Information section at the end of this article.

How to cite this article: Naser, A. N., Guiler, W., Lu, Q., & Chen, Y.-H. (2022). Nanoarchitecture and molecular interactions of epithelial cell junction proteins revealed by super-resolution microscopy. *Ann NY Acad Sci.*, *1516*, 175–187. https://doi.org/10.1111/nyas.14855